JOURNAL OF MAGNETIC RESONANCE **135,** 500–513 (1998)
ARTICLE NO. MN981603

Iterative Lineshape Fitting of MAS NMR Spectra: A Tool to Investigate Homonuclear *J* Coupling in Isolated Spin Pairs

Stephan Dusold,* Wolfgang Milius,† and Angelika Sebald*

**Bayerisches Geoinstitut and †Institut für Anorganische Chemie, Universität Bayreuth, D-95440 Bayreuth, Germany*

Received March 18, 1998; revised September 1, 1998

Possibilities and limitations of iterative lineshape fitting procedures of MAS NMR spectra of isolated homonuclear spin pairs, aiming at determination of magnitudes and orientations of the various interaction tensors, are explored. Requirements regarding experimental MAS NMR spectra as well as simulation and fitting procedures are discussed. Our examples chosen are the isolated ^{31}P spin pairs in solid $Na_4P_2O_7 \cdot 10H_2O$, (1), and $Cd(NO_3)_2 \cdot 2PPh_3$, (2). In both cases the two ^{31}P chemical shielding tensors in the molecular unit are related by C_2 symmetry, and determination of the orientations of these two tensors in the molecular frame is possible. In addition, aspects of homonuclear *J* coupling will be addressed. For 1, both magnitude and sign of $^2J_{iso}(^{31}P, ^{31}P)$ ($J_{iso} = -19.5 \pm 2.5$ Hz) are obtained; for 2, ($J_{iso} = +139 \pm 3$ Hz) anisotropy of *J* with an orientation of the *J*-coupling tensor collinear, or nearly collinear, with the dipolar coupling tensor can be excluded, while absence or presence of anisotropy of *J* with any other relative orientation of the *J*-coupling tensor cannot be determined.

Key Words: **solid-state NMR; magic-angle spinning; homonuclear spin pairs; spectral lineshape simulations; *J* coupling.**

INTRODUCTION

The Hamiltonian appropriate to describe an isolated, dipolar coupled homonuclear spin pair under MAS NMR conditions does not commute with itself at different times (it is homogeneous in the sense of Maricq and Waugh (*1*)). The theory describing the evolution of the density matrix for such isolated pairs of spin-$\frac{1}{2}$ nuclei has been fully described in the literature (*2–6*). Provided that numerically exact methods are employed for spectral lineshape simulations, combined with careful iterative fitting procedures, simple MAS NMR spectra of isolated homonuclear spin pairs offer an opportunity to simultaneously determine magnitudes and orientations of all interaction tensors present (chemical shielding, dipolar and *J* coupling) without having to carry out NMR experiments on oriented single crystals. Depending on the information wanted, the MAS NMR properties of isolated homonuclear spin pairs in polycrystalline powder samples may thus be exploited to determine the relative orientations of chemical shielding tensors, to derive internuclear distances, or to investigate aspects of isotropic and anisotropic properties of homonuclear *J* coupling.

In general, we will encounter two different categories of isolated homonuclear spin pairs. For spin pairs characterized by a large chemical shielding difference of the two spins (AX spin pairs), only MAS NMR spectra obtained at specific MAS frequencies, precisely matching a small integer multiple of the difference in isotropic chemical shielding of the two nuclei, have properties suitable for deriving orientational or distance information. This condition is known as rotational resonance (*6–10*) and has been used mainly for the determination of internuclear distances in ^{13}C spin systems (*11, 12*). With regard to homonuclear *J* coupling, away from any rotational resonance conditions, AX spin pairs allow determination of $|J_{iso}|$, where appropriate, either directly by inspection of the MAS NMR spectra or indirectly by applying pulse techniques designed for homonuclear *J* transfer under MAS conditions (*10, 13*). The MAS NMR properties of isolated homonuclear spin pairs with a small (AB spin pairs) or no (AA′ spin pairs) difference in the isotropic chemical shielding of the two nuclei are such that usually under a wide range of experimental conditions (MAS frequencies and external magnetic field strengths) spectral lineshapes, depending on magnitudes and orientations of all interaction parameters, will be observed (*14–17*). AA′ spin pairs, for which the two chemical shielding tensors are related by a symmetry operation other than inversion symmetry, represent a special case of rotational resonance ($n = 0$ rotational resonance). Numerically exact spectral lineshape simulations are necessary to determine the NMR parameters of AB and AA′ spin pairs from MAS NMR spectra, with the beneficial side effect that the absolute sign of the homonuclear *J* coupling constant may also be obtained in this way.

Here we will explore the practical possibilities and limitations of obtaining reliable and precise parameters from iterative fitting of spectral lineshapes of MAS NMR spectra of AA′ (and AB) spin pairs. We will consider quality requirements for the experimental NMR spectra as well as for the simulation and fitting procedures used. The practical examples chosen are the isolated homonuclear ^{31}P spin pairs in two crystalline solids of known single-crystal X-ray structure: $Na_4P_2O_7 \cdot 10H_2O$ (**1**) and $Cd(NO_3)_2 \cdot 2PPh_3$ (**2**). Both compounds already have a history

1090-7807/98 $25.00

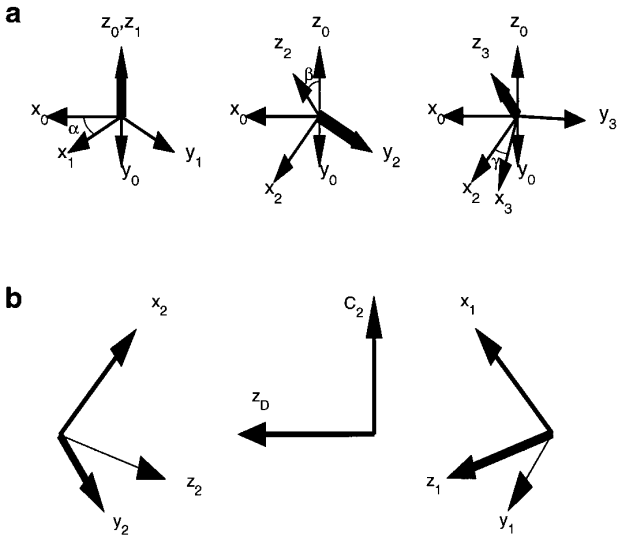

SCHEME 1. (a) Definition of Euler angles, α, β, γ relating, e.g., the chemical shielding to the dipolar coupling principal axis system; boldface arrows refer to the respective axis of rotation; see text for the definition of *x, y, z.* (b) Two chemical shielding tensors related by C_2 symmetry; boldface and thin arrows denote directions above and below the paper plane, respectively; see Eq. [4] for the corresponding relationships between the Euler angles for the two chemical shielding tensors.

as model cases for isolated homonuclear ^{31}P spin pairs (*14, 15, 18, 19*); here we will in particular address aspects of ^{31}P chemical shielding tensor orientations and of homonuclear J coupling $^2J(^{31}\text{P}, ^{31}\text{P})$. The P_2O_7 unit in **1** represents a case for which a J-coupling constant of small magnitude is to be expected, while for the ^{31}P spin pair in **2** the magnitudes of J and dipolar coupling constants are similar and raise the issue of possible anisotropy of J.

RESULTS AND DISCUSSION

Numerical Simulations and Iterative Fitting

The evolution of the density matrix for isolated homonuclear spin-$\frac{1}{2}$ pairs under MAS conditions, such as the ^{31}P spin pairs in **1** and **2,** has been investigated in detail in the literature (*2–6*). Only a short summary of the basic equations and results will be given here. The Hamiltonian of such a spin pair S_1–S_2 may be written as

$$H(t) = \omega_1(t)S_{1z} + \omega_2(t)S_{2z} + \omega_D(t) \times (2S_{1z}S_{2z} - \tfrac{1}{2}(S_{1+}S_{2-} + S_{1-}S_{2+})) + \omega_J S_1 S_2 + \omega_{J_{aniso}}(t)(2S_{1z}S_{2z} - \tfrac{1}{2}(S_{1+}S_{2-} + S_{1-}S_{2+})), \quad [1]$$

with ω_i (i = 1, 2) referring to chemical shielding (cs), ω_D to dipolar coupling, ω_J to isotropic coupling, and $\omega_{J_{aniso}}$ to anisotropic indirect coupling. The time dependence of each of the interactions may be expressed in terms of a Fourier series

$$\omega_\lambda(t) = \sum_{m=-2}^{2} \omega_\lambda^m \exp(im\omega_r t), \quad [2]$$

where ω_r is the spinning frequency in angular units and the coefficients take the form

$$\omega_\lambda^{(m)} = \omega_{iso}^\lambda \delta_{m0} + \delta_\lambda \left\{ D^2_{0,-m}(\Omega^\lambda_{PR}) - \frac{\eta_\lambda}{\sqrt{6}} [D^2_{-2,-m}(\Omega^\lambda_{PR}) + D^2_{2,-m}(\Omega^\lambda_{PR})] \right\} d^2_{-m,0}(\beta_{RL}); \quad [3]$$

$d^2_{-m,0}$ is a reduced Wigner element, and $D^2_{p,q}(\Omega^\lambda_{PR})$ is an element of the Wigner rotation matrix describing transformation from the principal axes system P of the interaction tensor through a crystal frame C to the rotor frame R. As a matter of convenience, the principal axes frame of the dipolar coupling interaction may be taken as coincident with the crystal frame, $\Omega^D_{PC} = (0, 0, 0)$. The definitions of the Euler angles describing the relative orientations of the chemical shielding and the dipolar coupling tensors, as well as the mutual symmetry relations of the Euler angles for two chemical shielding tensors related by C_2 symmetry, are illustrated in Scheme 1. For C_2 as the applicable symmetry operation the relationships of the Euler angles for the two chemical shielding tensors are

$$\alpha_2^{CS} = \alpha_1^{CS}, \quad \beta_2^{CS} = \beta_1^{CS} + \pi, \quad \gamma_2^{CS} = -\gamma_1^{CS} + \pi. \quad [4]$$

TABLE 1

^{31}P NMR Parameters for $Na_4P_2O_7 \cdot 10H_2O$, 1, and $Cd(NO_3)_2 \cdot 2PPh_3$, 2, Determined by Iterative Fitting of ^{31}P MAS NMR Spectra[a]

	1	**2**
σ_{iso} (ppm):	+2.3	−4.0
δ^{CS} (ppm):	−79 ± 1	−25 ± 1
η^{CS}:	0.35 ± 0.1	0.75 ± 0.1
α_1^{CS}(°):	−117 ± 4	20 ± 20
	−63 ± 4	160 ± 20
β_1^{CS}(°):	−23 ± 2	39 ± 5
γ_1^{CS}(°):	0 ± 6	−5 ± 10
$b_{12}/2\pi$ (Hz)[b]	−791	−242
J_{iso} (Hz)	−19.5 ± 2.5	+139 ± 3

[a] Symmetry-related angles α_2^{CS}, β_2^{CS}, γ_2^{CS} for the second ^{31}P chemical shielding tensor in **1** and **2** as defined in Eq. [4] and Scheme 1.

[b] Values calculated from the internuclear P–P distance, determined by single-crystal X-ray diffraction: r_{12} = 292 pm for **1** (*27*) and r_{12} = 433 pm for **2.**

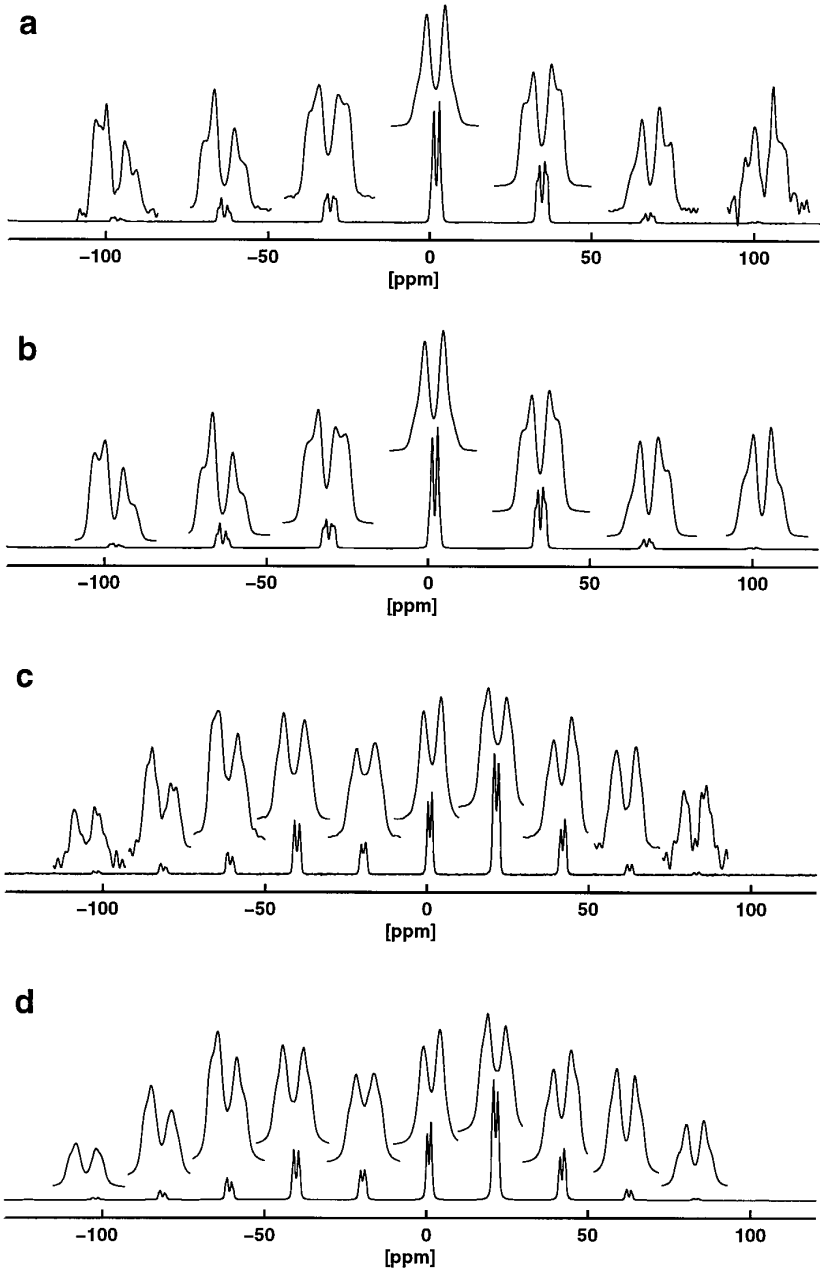

FIG. 1. Experimental and calculated ^{31}P MAS NMR spectra of $Na_4P_2O_7 \cdot 10H_2O$, **1,** corresponding to best-fit parameters given in Table 1. (a), (b) Experimental (a) and calculated (b) ^{31}P MAS NMR spectra of **1,** with $\omega_0/2\pi = -81.0$ MHz and $\omega_r/2\pi = 2656$ Hz. (c), (d) Experimental (c) and calculated (d) ^{31}P MAS NMR spectra of **1,** with $\omega_0/2\pi = -121.5$ MHz and $\omega_r/2\pi = 2503$ Hz. Insets give an expanded view of individual spinning sidebands of experimental and calculated spectra.

Note that for the particular case of C_2 symmetry relating the two chemical shielding tensors in the molecule no ambiguity regarding the orientation of the two chemical shielding tensors in the molecular frame exists (apart from the principal degeneracy that, in the absence of a third interacting spin, C_2 symmetry leaves the $1 \leftrightarrow 2$ assignment undetermined; see below): with the symmetry axis perpendicular to the dipolar axis direction *and* fixed in the molecular frame (in our case coplanar with the P–E–P plane and bisecting the P–E–P bond angle), no free rotation of the two chemical shielding tensors around the dipolar axis direction is possible. The difference $\gamma_1^{CS} - \gamma_2^{CS} = 2\gamma_1^{CS} - \pi$ depends on the magnitude of γ_1^{CS}, and correspondingly, the spectral lineshapes will depend on all Euler angles, α_i^{CS}, β_i^{CS}, γ_i^{CS}, and thus allow unambiguous determination of the chemical shielding tensor orientations in the molecular frame (*20*). The situation is different for cases where a mirror

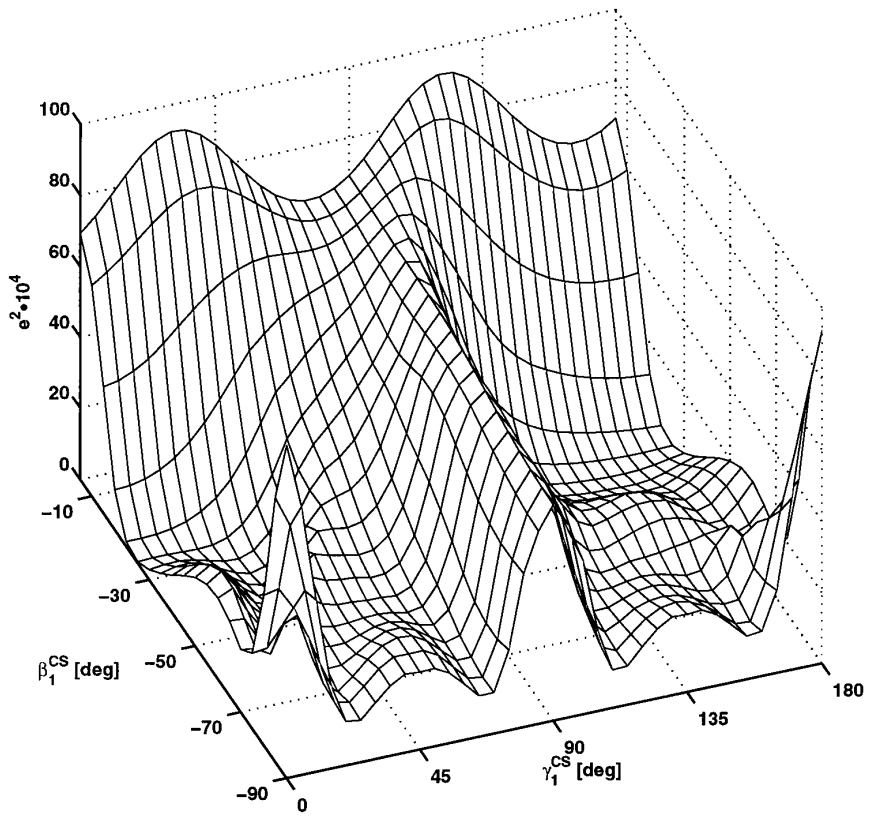

FIG. 2. Error plane, calculated for pair of fit parameters, Euler angles β_1^{CS}, γ_1^{CS}; calculation based on the experimental ^{31}P MAS NMR spectrum of **1** as shown in Fig. 1a with $\omega_0/2\pi = -81.0$ MHz and $\omega_r/2\pi = 2656$ Hz. The error e^2 is defined as $e^2 = 1/N \sum_{i=1}^{N} (S_{exp}(\omega_i) - S_{calc}(\omega_i))^2$, where $\max(S_{exp}(\omega_i)) = 1$.

plane, perpendicular to the dipolar axis direction, relates the two chemical shielding tensors. Then rotation of the two chemical shielding tensors around the dipolar axis direction is permitted, and the angle γ_i^{CS} cannot be determined from iterative lineshape fitting of MAS NMR spectra.

The isotropic part A_{iso}^{λ}, the anisotropy δ^{λ}, and the asymmetry parameter η^{λ} are related to the principal elements of the interaction tensor A^{λ} according to $A_{iso}^{\lambda} = (A_{xx}^{\lambda} + A_{yy}^{\lambda} + A_{zz}^{\lambda})/3$, $\delta^{\lambda} = A_{zz}^{\lambda} - A_{iso}^{\lambda}$, and $\eta^{\lambda} = (A_{yy}^{\lambda} - A_{xx}^{\lambda})/\delta_{\lambda}$ with $|A_{zz}^{\lambda} - A_{iso}^{\lambda}| \geq |A_{xx}^{\lambda} - A_{iso}^{\lambda}| \geq |A_{yy}^{\lambda} - A_{iso}^{\lambda}|$. We have $A_{iso}^{J} = \pi J_{iso}$, $A_{iso}^{D} = \eta^{D} = 0$, and $\delta^{D} = b_{12} = -\mu_0 \gamma_1 \gamma_2 \hbar/(4\pi r_{12}^3)$, where b_{12} denotes the dipolar coupling constant, γ_i $(i = 1, 2)$, refers to the gyromagnetic ratio of spins 1, 2, and r_{12} is the internuclear distance.

The powder spectrum $S(\omega)$ based on the Hamiltonian in Eq. [1] is the Fourier transform of

$$s(t) = \sum_{\Omega_{CR}} \mathrm{Tr}\{(S_1^+ + S_2^+)U(t, 0)(S_{1x} + S_{2x})U^{\dagger}(t, 0)\}. \quad [5]$$

Powder averaging is indicated by the summation, and the propagator U is related to the Hamiltonian by

$$U(t, 0) = \hat{T} \exp\{-i \int_0^t H(t')dt'\}, \quad [6]$$

where $\hat{T}$ is the Dyson time-ordering operator.

The most straightforward way to numerically calculate $S(\omega)$ would be the so-called direct method, that is, to calculate $s(t)$ directly by dividing the time evolution into small steps t_i, during which $H(t_i)$ may be considered as piecewise time independent. While this method provides an intuitive way to calculate $S(\omega)$, it is quite inefficient when high spectral resolution combined with a large-frequency bandwidth is required. In this case the calculation would have to be performed over a large number of steps (*2*). Hence, with a view to iterative fitting procedures for the determination of unknown parameters, the direct method will rarely be a good choice since fast simulation of $S(\omega)$ is a prerequisite for efficient fitting procedures. A faster method for calculation of the MAS NMR spectrum of a two-spin system is provided by the COMPUTE method (*21*), which employs a time-domain integration of the spin propagator over a single rotation period, while storing the intermediate results of this calculation. These are used in a succeeding

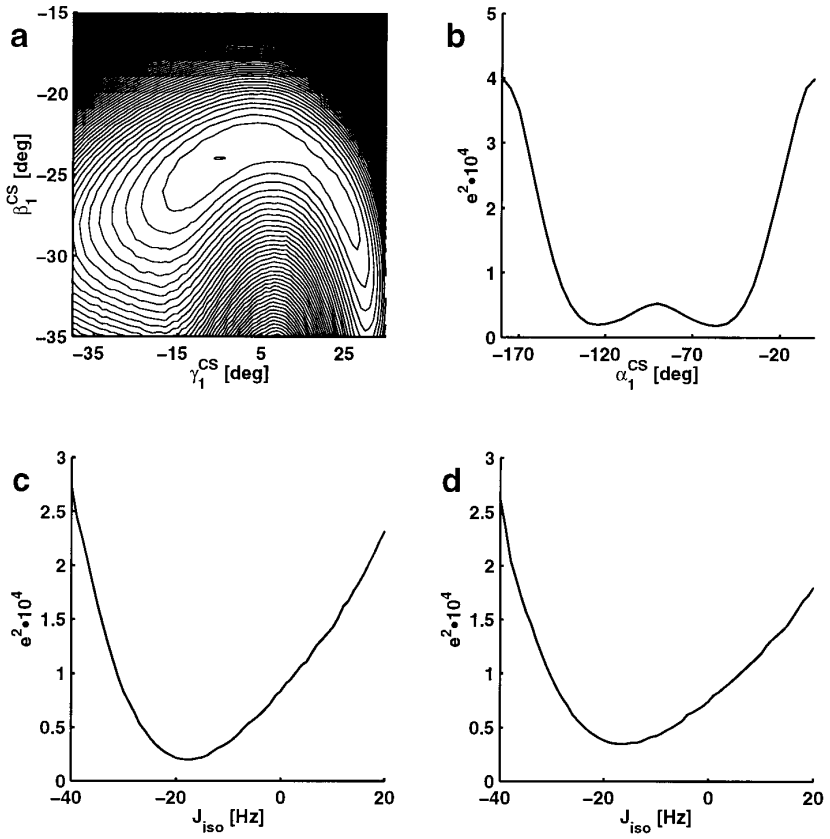

FIG. 3. Error scans for individual fit parameters of ^{31}P MAS NMR spectra of **1.** (a) Contour plot of minimum region of the β_1^{CS}, γ_1^{CS}-error plane shown in Fig. 2; contour levels are drawn at 0.19 as the minimum and at integer multiples thereof. (b) Scan for angle α_1^{CS}, (c) scan for J_{iso}; (a), (b), and (c) are based on the experimental spectrum shown in Fig. 1a ($\omega_0/2\pi = -81.0$ MHz and $\omega_r/2\pi = 2656$ Hz). (d) Scan for J_{iso}, based on an experimental spectrum with $\omega_0/2\pi = -121.5$ MHz and $\omega_r/2\pi = 3493$ Hz. Definition of e^2 as given for Fig. 2.

Fourier transformation step to calculate the amplitudes and associated frequencies of the spectral lines. Due to this restriction to a single rotation period, calculation of the resulting spectrum is fast but nevertheless with an effectively infinite frequency resolution.

The situation for the computation of the powder average is in some sense similar. Again, one could just imitate the physical behavior of the system by calculating a random distribution of crystallites. There are about 10^8 different crystallite orientations present in a typical sample (*22*), and, accordingly, the random distribution method is bound to be either a poor approximation or a highly inefficient one, depending on the number of different crystallite orientations one would calculate. Hence, the goal of numerous powder averaging methods (*23*) is to obtain a physically meaningful powder average while only having to consider a minimum number of different crystallite orientations, of the order 10^2 to 10^3. REPULSION (*24*) follows a numerical strategy by minimizing a potential function, in which way a very uniform distribution of orientational angles is achieved for relatively small numbers of crystallite orientations.

Another important question is the choice of optimization method, as this affects not only the speed but also the reliability of the fitting procedure. A large variety of algorithms, differing largely with respect to stability and speed, exists for the general problem of finding the global minimum of a function $y(x_1, x_2, \ldots, x_n)$ of n variables x_i $(i = 1, \ldots, n)$. There is no generally best method; the performance of all of them depends on the specific problem for minimization. Widely used are, for instance, the SIMPLEX algorithm or methods from the family of quasi-Newton methods (*25*). A convenient way to apply several of these methods for iterative fitting of NMR spectra is the MINUIT optimization package (*26*). It combines the possibility of executing different kinds of parameter analysis (scans, contours, calculation of correlations) with providing several different minimization methods. In accordance with the statements of the developers of MINUIT we find best performance with the Migrad method, a variation of the Davidon–Fletcher–Powell algorithm (*25*).

The general strategy chosen was to first fit multiple experimental NMR spectra, obtained at different external magnetic field strengths and MAS frequencies, assuming perfect exper-

imental parameters, and to check afterward whether imperfections of the experimental data—within their respective limits of inaccuracy—would have altered the results of the fits. This strategy is best if experimental errors can be expected to be small. A good indication for this regime will usually be that this "perfect experiment approximation" yields good fits with identical parameters for experimental spectra obtained under different experimental conditions.

*^{31}P MAS NMR Spectra of $Na_4P_2O_7 \cdot 10H_2O$, **1***

The single-crystal X-ray structure of **1** (*27*) provides information on the internuclear P–P distance and the P–O–P bond angle in the P_2O_7 unit. The symmetry operation relating the two ^{31}P chemical shielding tensors in the P_2O_7 unit is known to be a C_2 axis, bisecting the P–O–P bond angle. Using the distance and symmetry information from single-crystal X-ray diffraction as known and fixed parameters for iterative fitting of various ^{31}P MAS NMR spectra of **1,** we find good agreement of all parameters from all fits (see Table 1 for best-fit parameters), in accordance with the "perfect experiment approximation." A comparison of two different experimental ^{31}P MAS NMR spectra of **1** with the corresponding calculated (best-fit parameters) NMR spectra is shown in Fig. 1. Even the interaction with by far the smallest magnitude (J_{iso}) is defined within a narrow range, $J_{iso} = -19.5 \pm 2.5$ Hz.

Beyond this statement of obtaining good final agreement between experimental and calculated spectra, a careful exploration of possible pitfalls and limitations seems in order. The first point to address is the sensitivity of the fits with regard to the various individual parameters, especially for parameters of small magnitude and for strongly correlated parameters. There are several options: we may scan through the individual parameters while keeping the remaining fit parameters fixed, we may perform additional fits where the parameter under inspection is forced to lie outside the minimum range previously found in unrestricted fits, and we may calculate error planes for pairwise combinations of strongly correlated parameters. For the spin pairs considered here, the Euler angles β_i^{CS} and γ_i^{CS} represent a pair of strongly correlated parameters, both with high impact on the spectral lineshapes. In fact, calculations of error planes for pairs of fit parameters turn out an important ingredient in the overall fit procedure. From calculating β_1^{CS}, γ_1^{CS}-error planes for various ^{31}P MAS NMR spectra of **1** (see Figs. 2 and 3a), we find that both angles $\beta_1^{CS} = -23 \pm 2°$ and $\gamma_1^{CS} = 0 \pm 6°$ are well defined, with high sensitivity. For **1,** β_1^{CS} describes the angle between the *least* shielded tensor component and the unique axis of the dipolar coupling tensor. The lesser sensitivity for $\alpha_1^{CS} = -117 \pm 4°$ (see Fig. 3b) arises also as a consequence of the asymmetry parameter $\eta^{CS} = 0.35 \pm 0.1$, not deviating much from axial symmetry for the ^{31}P chemical shielding tensors in **1.** By arbitrarily choosing one of the two possible $1 \leftrightarrow 2$ assignments, the set of angles α_1^{CS}, β_1^{CS}, γ_1^{CS} determined for **1** describes the following orientations of the ^{31}P chemical shielding tensors in the P_2O_7 unit. $\gamma_1^{CS} = 0 \pm 6°$ renders the least shielded tensor component coplanar with the molecular P–$O_{central}$–P plane, and $\beta_1^{CS} = -23 \pm 2°$ then corresponds to the least shielded tensor component collinear with the molecular P–$O_{central}$ bond direction, while the most shielded tensor component is oriented perpendicular to the molecular P–$O_{central}$–P plane. These results from iterative fitting of ^{31}P MAS NMR spectra of **1** are supported by the findings of an earlier single-crystal NMR study on α-$Ca_2P_2O_7$ (*28*). Also shown in Fig. 3 (see Figs. 3c and 3d) are scans of J_{iso} for fits of two different experimental ^{31}P MAS NMR spectra of **1.** While, in accordance with the small magnitude of this parameter, the sensitivity of the fits to J_{iso} is much reduced in comparison with, e.g., the angle β_1^{CS}, the scans of J_{iso} still display defined minima in good mutual agreement. Note that the scans imply a negative sign for J_{iso} and that, in this particular case, the sensitivity is not inferior to the sensitivity for α_1^{CS}. Given that the smallest of all contributions to the calculated spectral lineshapes is the effect of J_{iso}, we have to

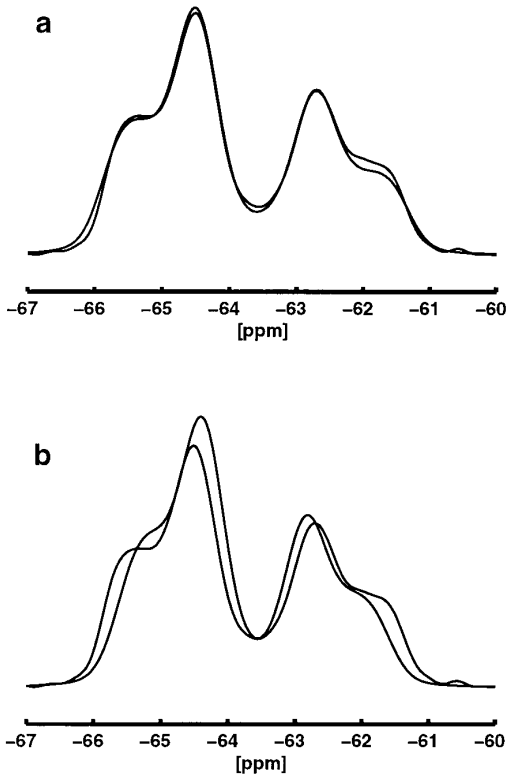

FIG. 4. Effect of sign of J_{iso}, illustrated for the second-order (−2) spinning sideband in the ^{31}P MAS NMR spectrum of **1** as shown in Fig. 1a with $\omega_0/2\pi = -81.0$ MHz and $\omega_r/2\pi = 2656$ Hz. (a) Experimental and calculated lineshape, corresponding to best-fit parameters ($J_{iso} = -19.5 \pm 2.5$ Hz) where J_{iso} was a free fit parameter, plotted on top of each other; b): experimental and calculated lineshape, corresponding to best-fit parameters where J_{iso} was fixed to $J_{iso} = +19.5$ Hz, plotted on top of each other. All fits with J_{iso} merely restricted to $J_{iso} > 0$ converged toward $J_{iso} = 0$.

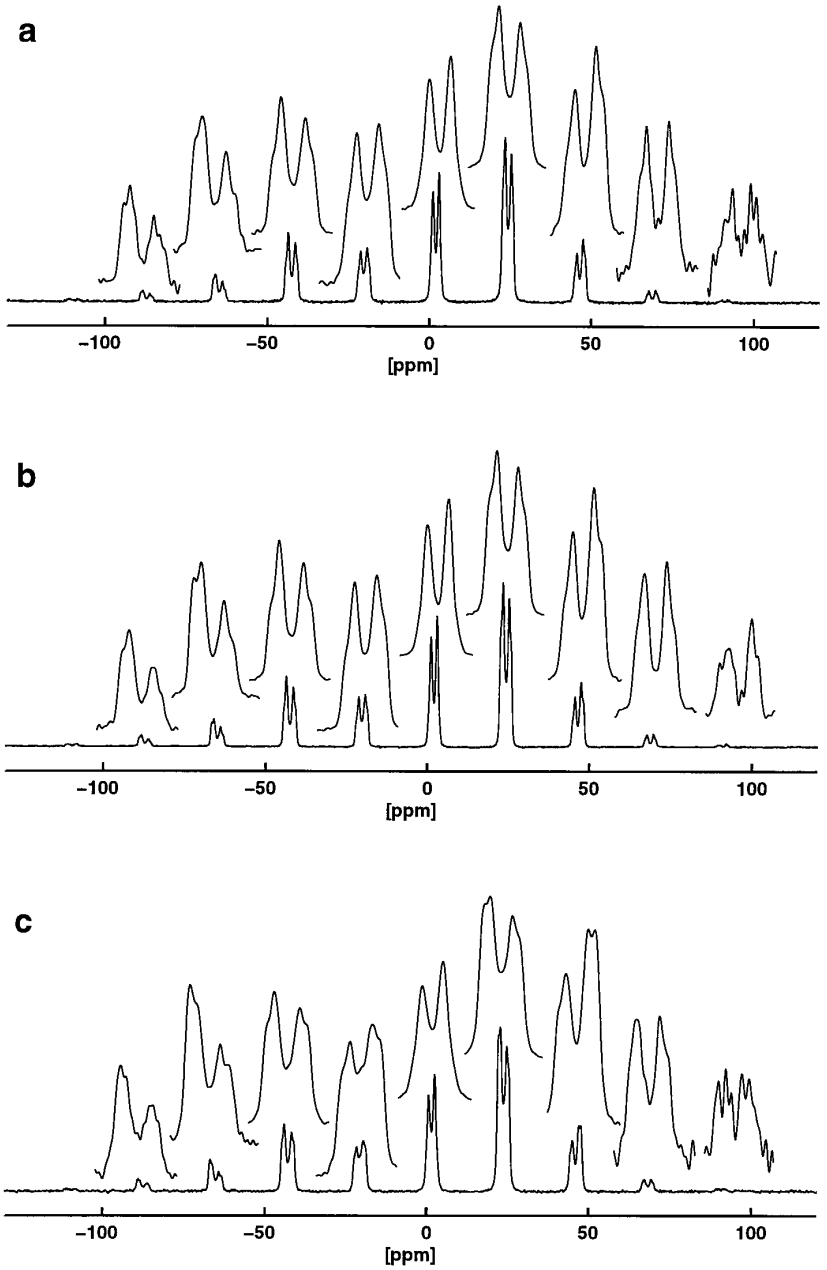

FIG. 5. Experimental ^{31}P MAS NMR spectra of **1,** with $\omega_0/2\pi = -81.0$ MHz and $\omega_r/2\pi = 1807$ Hz. (a), (b) ^{31}P MAS NMR spectra of a very finely ground sample of **1,** obtained with single-pulse ^{31}P excitation (a) and with cross polarization (b). (c) ^{31}P CP MAS NMR spectrum of a slightly less finely ground sample of **1.**

further investigate the possibility that only a local, false minimum for J_{iso} may have been found. Additional fits with J_{iso} fixed to zero, or with J_{iso} restricted to $J_{iso} > 0$, help to exclude this possibility and to further confirm both sign and magnitude of J_{iso}. The final errors of such restricted fits are found to be inferior to the minimized errors obtained from fits where J_{iso} is unrestricted with respect to magnitude and sign; in particular, the fine structure of individual spinning sidebands is not sufficiently well reproduced by these restricted fits, as is illustrated in Fig. 4.

Up to this point, we are still implicitly operating within the assumption of sufficiently "perfect" experimental NMR data. Hence, our next step *a posteriori* has to justify this assumption by discussing the influence experimental imperfections would have had on the final fit results. As a matter of completeness we should mention the prerequisites of stable MAS frequencies

within ±2 Hz and of an optimized B_0 homogeneity. Shimming the probe such that ^{13}C MAS NMR spectra of a full rotor with adamantane yield undistorted ^{13}C resonance lineshapes with a width at half height not exceeding 3 Hz (e.g., at $B_0 = 7$ T) is necessary: slightly less optimized B_0 homogeneity already leads to a loss of fine structure in the various spinning sidebands of ^{31}P MAS NMR spectra of **1.** Another practical matter of optimization concerns the adjustment of the magic angle. We find that the very sharp ^{31}P MAS NMR resonances of isolated magnetically equivalent ^{31}P spin pairs, such as, for instance, in tetraethyldiphosphine disulfide (*29*), allow very accurate setting of the magic angle. Another possible, and not entirely unlikely, source of distortion of the spectral lineshapes in experimental ^{31}P MAS NMR spectra might be the use of cross polarization (CP). Possible spectral lineshape distortions caused by CP can be excluded for **1:** within experimental error ^{31}P MAS NMR spectra, obtained by conventional Hartmann–Hahn cross polarization and by direct single-pulse ^{31}P excitation, display identical spectral lineshapes (see Figs. 5a and 5b). All our ^{31}P MAS NMR spectra have been obtained from a very finely ground sample of **1.** Trivial as it may seem at first glance, this aspect of sample quality is of practical importance with respect to reliable lineshape fitting procedures. An "imperfect powder average" in the rotor, caused by the presence of only a few, slightly coarser grains in the sample, is sufficient to yield misleading spectral lineshapes (see Fig. 5c). That it may only take a minor powder imperfection of the sample for such distortion effects to occur is illustrated by the following gedankenexperiment. Suppose we have a rotor, containing a perfect powder sample with 10^8 crystallite orientations, to which we add one crystallite in one particular orientation. The size of this crystallite amounting to 1% of the sample misadjusts the weighting factor for this particular orientation to 10^{-2} instead of 10^{-8}. In short, if we wish to be able to significantly determine J parameters of small magnitudes from MAS NMR spectra, we have to avoid as much as possible all contributions from experimental imperfections which would generate losses of sensitivity or precision in the iterative fitting procedures.

Finally, we need to compare our results on **1** to previously obtained ^{31}P NMR parameters for this compound. Magnitudes and orientations of the ^{31}P chemical shielding tensors of **1,** now determined by numerically exact spectral lineshape simulations, agree within error limits with these parameters for **1** obtained earlier from various other approaches (*14, 15, 18, 30*). However, previously neither magnitude nor sign of J_{iso} could be determined for **1** (*14, 15, 18*). Our finding of $J_{iso} = -19.5 \pm 2.5$ Hz for **1** agrees well with the results of ^{31}P TOBSY experiments (*13*) on the P_2O_7 units in solid $Cd_2P_2O_7$ (^{31}P AB spin pair, $|J_{iso}| = 23 \pm 4$ Hz (*15*)) and in the pseudo-cubic phase of SiP_2O_7 (^{31}P AB and AX spin pairs, $|J_{iso}|$ ranging from 17 to 23 Hz (*31*)).

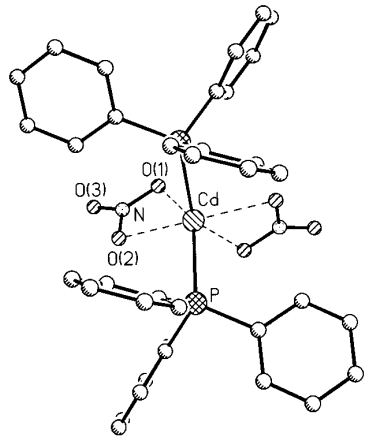

FIG. 6. Molecular structure of $Cd(NO_3)_2 \cdot 2PPh_3$, **2,** as determined by single-crystal X-ray diffraction. Selected bond lengths (pm) and bond angles (°): Cd–P 259.2(1), Cd–O(1) 243.7(3), Cd–O(2) 237.5(2), N–O(1) 123.9(3), N–O(2) 126.2(4), N–O(3) 120.7(4); P–Cd–P′ 113.3(1), O(1)–N–O(3) 122.3(3), O(1)–N–O(2) 115.8(3), O(2)–N–O(3) 121.9(3).

^{31}P MAS NMR Spectra of $Cd(NO_3)_2 \cdot 2PPh_3$, 2

From a chemical point of view, **1** and **2** have very little in common. Viewed from the properties of their respective ^{31}P spin systems, **1** and **2** are more closely related: the two P atoms are separated by two chemical bonds in a nonlinear P–E–P arrangement; the two ^{31}P chemical shielding tensors are related by symmetry (C_2 axis, see below) and represent the interaction with the largest magnitude within the spin pair. Distinct differences between **1** and **2** concern δ^{CS} (**1**) > δ^{CS} (**2**), η^{CS} (**1**) < η^{CS} (**2**), and $|J_{iso}|$ (**1**) < $|J_{iso}|$ (**2**). An earlier report of ^{31}P MAS NMR spectra of $Cd(NO_3)_2 \cdot 2PPh_3$, **2** (*19*) gave an estimate for $|J_{iso}| = 131 \pm 7$ Hz and predicted the two ^{31}P chemical shielding tensors in the molecule to be related by a C_2 symmetry axis, with the σ_{22} components of the chemical shielding tensors supposedly oriented near the Cd–P bond directions. The magnitude of J_{iso} and the geometry of the P–Cd–P fragment in **2** are such that this ^{31}P spin pair appears a suitable object for a more detailed search of possible contributions from anisotropy of J by means of iterative fitting of ^{31}P MAS NMR spectra of **2.**

In order to be able to operate on safe grounds concerning the molecular symmetry and internuclear distances, it is desirable, if not necessary, to know the single-crystal X-ray structure of **2.** $Cd(NO_3)_2 \cdot 2PPh_3$ crystallizes in space group $C2/c$; the two P sites in the molecule are crystallographically equivalent and related by a twofold axis of symmetry, with an internuclear P–P distance of 433 pm (corresponding to $b_{12}/2\pi = -242.4$ Hz) and a P–Cd–P bond angle of 113.3°. Figure 6 shows a plot of the molecular structure of **2.**

The following discussion of the ^{31}P MAS NMR spectra of **2** only takes into account the spectral contributions from those

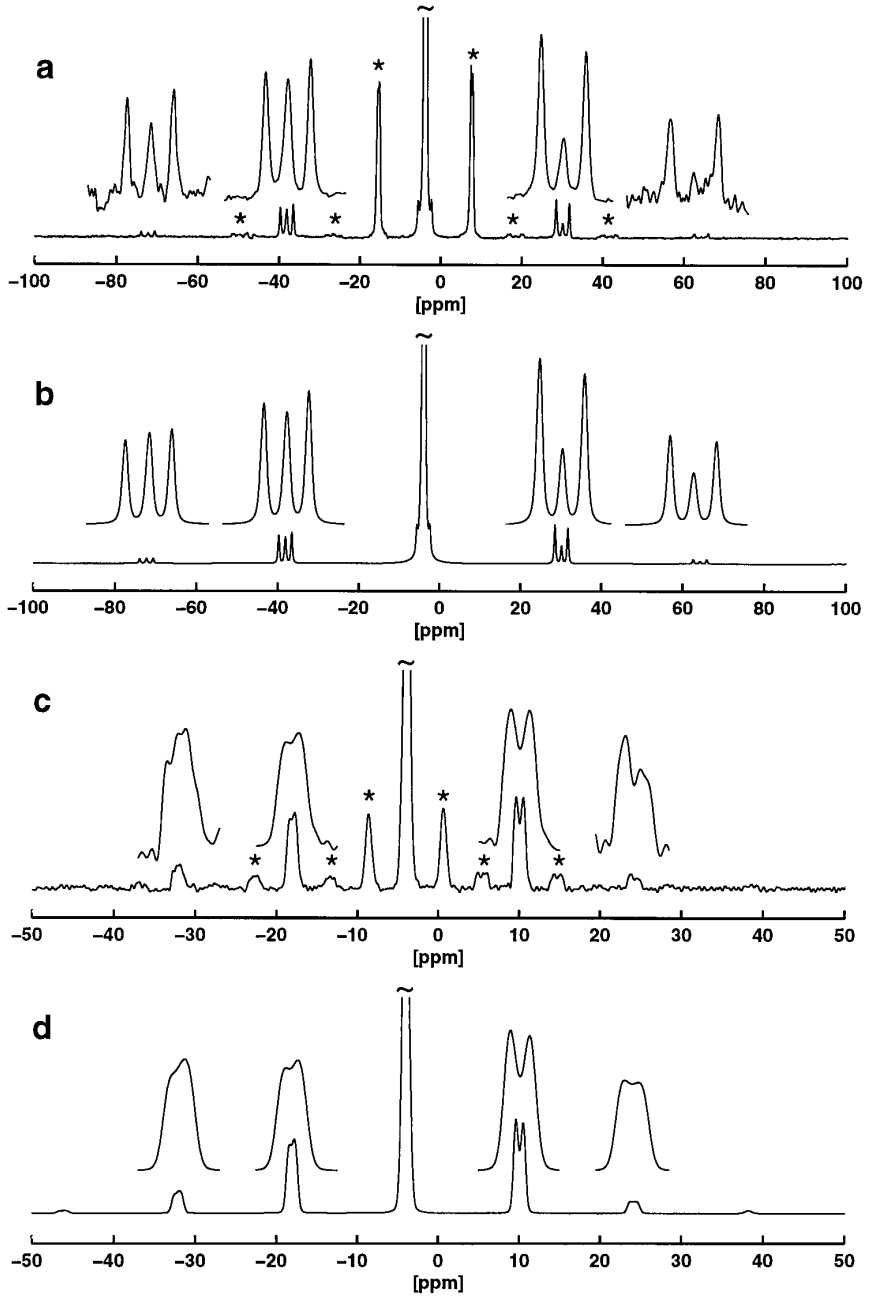

FIG. 7. Experimental and calculated ^{31}P MAS NMR spectra of $Cd(NO_3)_2 \cdot 2PPh_3$, **2,** corresponding to best-fit parameters given in Table 1. (a), (b) Experimental (a) and calculated (b) ^{31}P MAS NMR spectra of **2,** with $\omega_0/2\pi = -81.0$ MHz and $\omega_r/2\pi = 2767$ Hz. (c), (d) Experimental (c) and calculated (d) ^{31}P MAS NMR spectra of **2,** with $\omega_0/2\pi = -202.5$ MHz and $\omega_r/2\pi = 2851$ Hz. Insets give an expanded view of individual spinning sidebands of experimental and calculated spectra. In the experimental spectra (a), (c), * indicate satellites due to minority $^{111}Cd(^{31}P)_2$ and $^{113}Cd(^{31}P)_2$ isotopomers; the intense zeroth-order spinning sideband is shown truncated in all spectra.

(majority) isotopomers of **2** representing an isolated ^{31}P spin pair; the properties of (minority) three-spin system isotopomers $^{113}Cd(^{31}P)_2$, $^{111}Cd(^{31}P)_2$ in fragments CdP_2 such as in **2** are described elsewhere (*32*). The best-fit ^{31}P NMR parameters for **2** are given in Table 1. In Fig. 7 the corresponding simulations are compared to two experimental ^{31}P MAS NMR spectra of **2.**

The value of δ^{CS} for the ^{31}P chemical shielding tensors in **2** is smaller by approximately a factor of three than in **1.** Even in the ^{31}P MAS NMR spectrum of **2** obtained at an external magnetic field strength $B_0 = 11.8$ T and at the lowest possible MAS frequency for which no overlap problems occur, the amplitude of the zeroth-order spinning sideband is nearly five

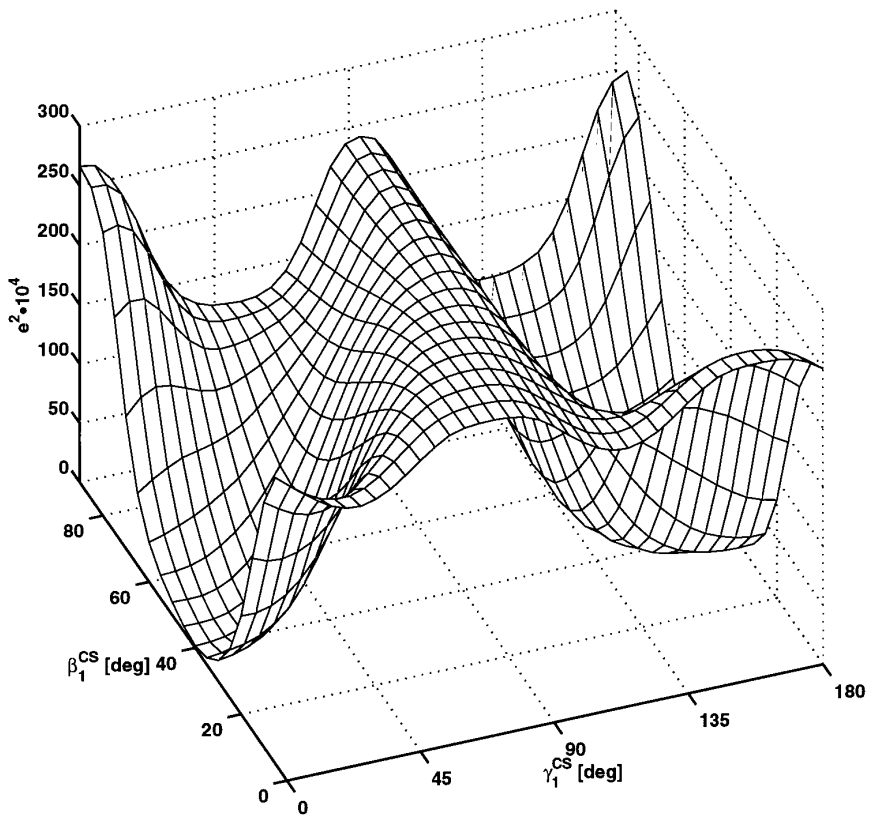

FIG. 8. Error plane, calculated for pair of fit parameters, Euler angles β_1^{CS}, γ_1^{CS}; calculation based on an experimental ^{31}P MAS NMR spectrum of **2** with $\omega_0/2\pi = -121.5$ MHz and $\omega_r/2\pi = 1413$ Hz. The error e^2 is defined as for Fig. 2.

times larger than the amplitudes of the first-order spinning sidebands. Obviously, we have to operate in a less than optimum experimental regime and need to specify the accuracy of the ^{31}P chemical shielding tensor parameters for **2.** Despite the necessarily nonideal experimental conditions, the Euler angles β_1^{CS} and γ_1^{CS} again represent sensitive and strongly correlated fit parameters (see Figs. 8 and 9a), and both $\delta^{CS} = -25.0 \pm 1.0$ ppm and $\eta^{CS} = 0.75 \pm 0.1$ are well defined, with good sensitivity, as is shown in Figs. 9b and 9c. We find one fairly narrow minimum region for $\beta_1^{CS} = 39 \pm 5°$ and $\gamma_1^{CS} = -5 \pm 10°$. The scan for α_1^{CS} shows a broad minimum region for $\alpha_1^{CS} = 20 \pm 20°$, with the steep ascent of the error curve safely excluding all angles $\alpha_1^{CS} > 40°$ (see Fig. 9d). For **2,** $\beta_1^{CS} = 39 \pm 5°$ describes the orientation of the *least* shielded tensor component to the direction of the unique component of the dipolar coupling tensor. If we wish to relate this information to the molecular frame of **2,** we are again faced with the principal $1 \leftrightarrow 2$ assignment uncertainty. One of the two possible options would correspond to an orientation of the least shielded ^{31}P tensor component nearly coincident (within 6°) with the molecular Cd–P bond direction and with the intermediate shielding tensor component nearly perpendicular to the P–Cd–P plane. The second possible option again renders the most and the least shielded tensor components nearly coplanar with the P–Cd–P plane, with an angle of 24° between the Cd–P bond direction and the most shielded tensor component. The set of values for α_1^{CS}, β_1^{CS}, γ_1^{CS} determined for **2** thus only excludes the intermediate shielding tensor components from being oriented close to the Cd–P bond directions. A resolution of these orientational uncertainties for the ^{31}P chemical shielding tensor components in the molecular frame would require to include information derived from taking a third interacting spin into account (*32*). In the absence of such information, we can only qualitatively argue that, in analogy to the results of a ^{31}P single-crystal NMR study on a closely related mercury complex, $Hg(NO_3)_2 \cdot 2PPh_3$ (*33*), an orientation of the most shielded tensor component near the Cd–P bond direction also in **2** may appear the more likely circumstance.

Other than for **1,** we find for **2** that, owing to its magnitude, J_{iso} can be regarded immediately as a well-defined parameter ($J_{iso} = +139 \pm 3$ Hz). The scan for J_{iso} (see Fig. 10a) shows a clearly smaller error for $J_{iso} > 0$ than for $J_{iso} < 0$. The question arises of whether we may neglect possible contributions from anisotropy of J for **2.** Only if the tensor describing the anisotropy of J is collinear with the dipolar coupling tensor and if its asymmetry parameter $\eta^J = 0$ may an effective dipolar coupling constant $|b_{eff}| = b_{12} \pm \frac{1}{2}\delta^J$ be defined (*18, 34*) from which δ^J may be directly obtained. If this

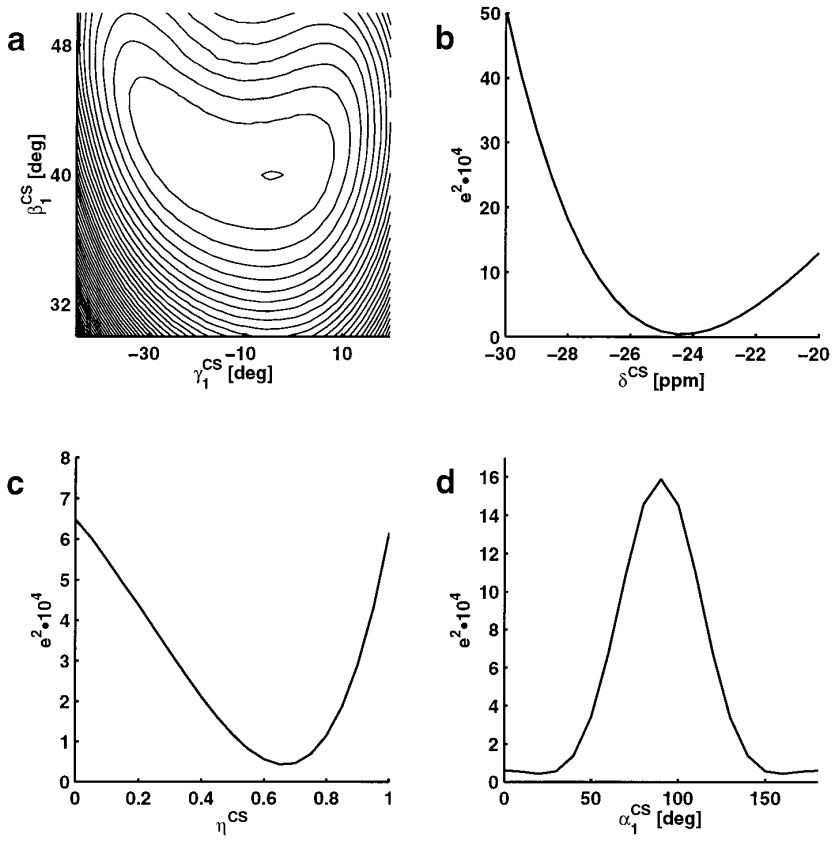

FIG. 9. Error scans for individual fit parameters of ^{31}P MAS NMR spectra of **2,** based on the experimental ^{31}P MAS NMR spectrum with $\omega_0/2\pi = -202.5$ MHz and $\omega_r/2\pi = 2851$ Hz as shown in Fig. 7c. (a) Contour plot of the minimum region of the β_1^{CS}, γ_1^{CS}-error plane shown in Fig. 8. Contour levels are drawn at 1.56 as the minimum and at integer multiples thereof; and error scans for (b) δ^{CS}, (c) η^{CS}, (d) angle α_1^{CS}. e^2 is defined as for Fig. 2.

condition does not hold, obviously a full calculation (Eq. [1]) including angles, η^J, and δ^J is necessary. However, also in this case for non-negligible J_{aniso} we may still find a (somewhat loosely defined) pseudo-b_{eff} from iterative fits where J_{aniso} is not explicitly included, but where the dipolar coupling constant is a free fit parameter. We then may take a significant deviation of pseudo-b_{eff} from b_{12}, as calculated from the known internuclear distance, as an indication for the presence of J_{aniso}. With possibly non-negligible J_{aniso} in mind, we inspect more closely the corresponding fit parameters. Figure 10b shows the scan for b_{12}, resulting from a fit where b_{12} served as a free fit parameter but where J_{aniso} was not explicitly included. The minimum range found for $b_{12}/2\pi = -240 \pm 20$ Hz (corresponding to an internuclear P–P distance of 435 $\pm$ 12 pm) is centered precisely at the value for $b_{12}/2\pi = -242.4$ Hz, calculated from the internuclear P–P distance in **2** as determined by single-crystal X-ray diffraction ($r_{12} = 433$ pm). Furthermore, despite now having used an additional fit parameter, neither do the final errors of this fit improve significantly (<8%) in comparison to fits where b_{12} was a fixed parameter, nor do we find a significant change of any of the other parameters. We might stop at this point, concluding that J_{aniso} plays no significant role for the ^{31}P spin pair in **2.** However, given that the symmetry of the P–Cd–P fragment in **2** excludes the assumption of a well-defined b_{eff}, this conclusion leaves an unsatisfying aftertaste. The results of fits with $b_{12}/2\pi = -242.4$ Hz as a fixed parameter, but taking J_{aniso} fully into account according to the complete Hamiltonian in Eq. [1], are shown in Figs. 10c and 10d. Introduction of this additional term as free fit parameters does not lead to further improvement of errors e^2. The sensitivity of these fits to δ^J, however, strongly depends on the orientation of the J-coupling tensor to the dipolar principal axes system. If the orientation of the J-coupling tensor is arbitrarily chosen collinear with the unique axis of the dipolar-coupling tensor, then a scan through δ^J essentially mirrors a scan through b_{12}, even for $\eta^J \neq 0$ with a well-defined minimum at $\delta^J = 0 \pm 50$ Hz (see Fig. 10c). The situation is different for orientations of the J-coupling tensor not collinear with the dipolar-coupling tensor: scans through δ^J then show a very low sensitivity for this parameter (see Fig. 10d), precluding the determination of its magnitude. We may conclude for **2** that we can exclude a large anisotropy

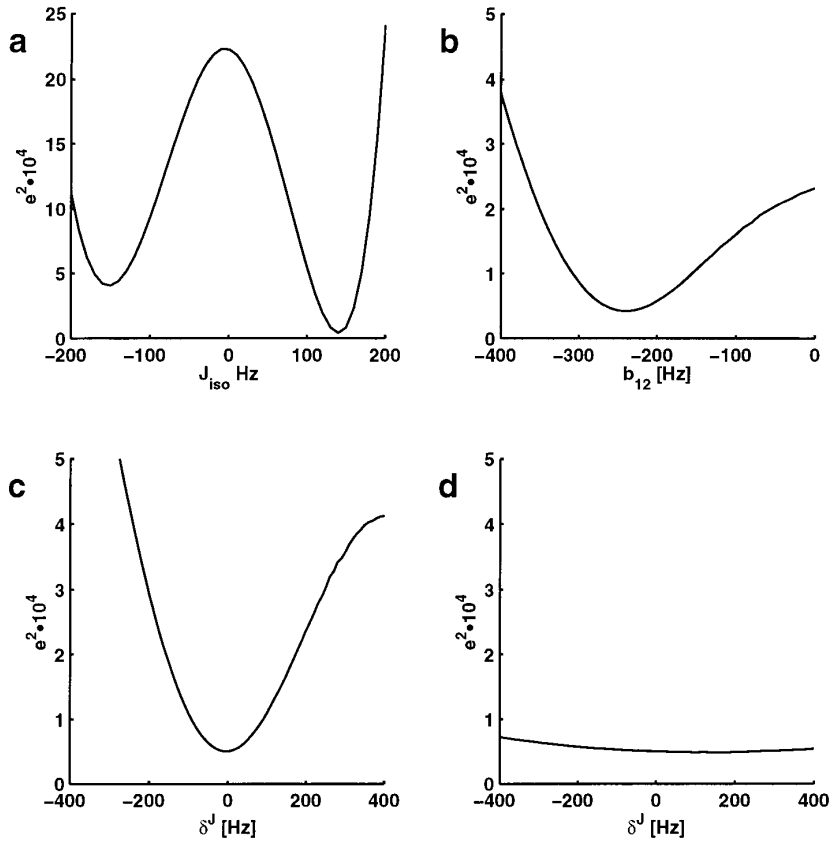

FIG. 10. Error scans for individual fit parameters, based on the experimental ^{31}P MAS NMR spectrum of **2** with $\omega_0/2\pi = -202.5$ MHz and $\omega_r/2\pi = 2851$ Hz as shown in Fig. 7c; e^2 as defined for Fig. 2. Error scans for (a) J_{iso} (from fit with b_{12} fixed to the value calculated from the internuclear P–P distance, and not including J_{aniso}); (b) b_{12} (but not including J_{aniso}); (c), (d) δ^J (all other parameters as given in Table 1); the asymmetry parameter of the anisotropy of J was $\eta^J = 0.5$, and the Euler angles describing the orientation of the J-coupling tensor in the dipolar axes system were $\alpha^J = \beta^J = \gamma^J = 0°$ (c) and $\alpha^J = 12°$, $\beta^J = 43°$, $\gamma^J = 0°$ (d), respectively.

of the J-coupling tensor collinear with the dipolar-coupling tensor. Accordingly, we would have determined the correct internuclear P–P distance for **2** also in the absence of knowledge of the single-crystal X-ray structure. We cannot exclude anisotropy of J coupling for **2** in a more general sense: there still might be considerable anisotropy with an orientation of the J-coupling tensor such that this parameter becomes "invisible" from our experimental ^{31}P MAS NMR data (*35*).

EXPERIMENTAL

Compounds

Compound **1,** $Na_4P_2O_7 \cdot 10H_2O$, is commercially available (Aldrich Chemicals) and has been used without further purification. Compound **2,** $Cd(NO_3)_2 \cdot 2PPh_3$, is obtained from the reaction of one equivalent of $Cd(NO_3)_2 \cdot 4H_2O$ with two equivalents of PPh_3 in refluxing EtOH under inert gas atmosphere. The crude product **2** precipitates upon fast cooling of the EtOH solution. After drying, the crude product is redissolved in the minimum amount of hot EtOH; large single crystals of pure **2** grow from the slowly cooled solution. From this yield of single crystals of **2,** several crystals suitable for X-ray diffraction have been selected; the remainder of the material has been used, after grinding it, for ^{31}P MAS NMR experiments.

Single-Crystal X-Ray Diffraction

A colorless crystal, suitable for X-ray structure determination, was irregularly shaped and of dimension $0.35 \times 0.18 \times 0.15$ mm. $C_{36}H_{30}N_2O_6P_2Cd$ (**2**) crystallizes in the monoclinic space group $C2/c$ (Nr.15) with the lattice parameters $a = 13.748(2)$, $b = 13.837(2)$, $c = 18.021(2)$ Å, $\beta = 95.47(2)°$, and $Z = 4$. The unit cell volume is 3412.6(8) Å^3, and the absorption coefficient 0.781 mm^{-1}. The intensities of 7937 reflections in the range 3°–55° (2ϑ) were measured on a Siemens P4 diffractometer with Mo$K\alpha$ radiation ($\lambda = 0.71073$ Å) in the ω-scan mode. After merging, 3918 unique reflections remained, and 3280 reflections were assigned to be observed ($F_0 \geq \sigma(F_0)$). The intensity data were

corrected for absorption on the basis of the Ψ-scans of 10 different reflections. The min/max transmission factors are 0.4168/0.4460. After Lorentz and polarization correction, the structure was solved by applying direct methods (SHELXTL PLUS V.4.2) (*36*), yielding Cd, P, and some lighter atoms, and by subsequent Fourier syntheses. The matrix least-squares refinement with 214 parameters converged at *R*/*wR* values of 0.032/0.030. The max/min residual electron density is 0.45/−0.44 e Å^{-3}. Crystallographic data (excluding structure factors) for the structure reported in this paper have been deposited with the Cambridge Crystallographic Data Centre as supplementary publication no. CCDC - 103049. Copies of the data can be obtained free of charge on application to the Director, 12 Union Road, Cambridge CB2 1EZ, UK (fax: int.code(1223)336-033; e-mail: deposit@chemcrys.cam.ac.uk).

NMR Experiments

^{31}P MAS NMR spectra of **1** and **2** were obtained using Hartmann–Hahn CP with CP contact times of 3 ms and recycle delays of 10 s for **1,** and 1.5 ms and 40–60 s for **2,** respectively. ^{31}P MAS NMR spectra of **1** and **2** were recorded on Bruker MSL 100, MSL 200, MSL 300, and DSX 500 NMR spectrometers, corresponding to ^{31}P Larmor frequencies of −40.5, −81.0, −121.5, and −202.5 MHz, respectively. Standard double-bearing probes and ZrO_2 rotors (4 and 7 mm diameter) were used; spinning frequencies were in the range 1.5–7.0 kHz and were actively controlled to within ±2 Hz using home-built equipment. ^{31}P chemical shielding is given relative to external 85% H_3PO_4, σ_{iso} ^{31}P = 0 ppm.

Shielding notation (*37*) is used throughout, and anisotropy parameters are reported according to Haeberlen's convention (*38*). Care was taken to choose combinations of the experimental parameters external magnetic field strength and MAS frequency (*39*) optimized for purposes of iterative lineshape fitting procedures. Experimental linebroadening was simulated by folding the spectrum either with an exponential function only or with an exponential and a Gaussian function. Both methods yielded identical parameters within error limits, with a general tendency that additional Gaussian linebroadening improves the visual agreement between experimental and calculated spectral lineshapes. All simulation and fitting programs utilized the GAMMA programming package (*40*). COMPUTE (*21*) was used for calculating all MAS NMR spectra, with n = 6–20 and n' = 2–8 (n, n' as defined in (*21*)). Powder averaging involved 232 different sets of angles α_{CR} and β_{CR}, selected according to REPULSION (*24*), and 20–40 different angles γ_{CR}. Typical times required for calculation of one spectrum were 20 to 60 s on Silicon Graphics O2 and Indy workstations. Note that using a recently introduced improved COMPUTE approach (*41*) further reduces the time required for the calculation of one spectrum to ca. 2 s (*32*). The Migrad method from the MINUIT optimization package (*26*) was used for minimization of e^2.

ACKNOWLEDGMENTS

Support of this work by the Deutsche Forschungsgemeinschaft and the Fonds der Chemischen Industrie is gratefully acknowledged. We thank S. Steuernagel, Bruker Analytische Messtechnik, Rheinstetten, for providing −202.5 MHz ^{31}P MAS NMR spectra of **2.**

Note added in proof. The results of a recent ^{31}P single-crystal NMR study of $Cd(NO_3)_2 \cdot 2PPh_3$, **2,** agree well with the ^{31}P NMR parameters derived from iterative fitting of ^{31}P MAS NMR spectra of **2** (42).

REFERENCES

1. M. M. Maricq and J. S. Waugh, NMR in rotating solids, *J. Chem. Phys.* **70,** 3300–3316 (1979).
2. M. H. Levitt, D. P. Raleigh, F. Creuzet, and R. G. Griffin, Theory and simulations of homonuclear spin pairs in rotating solids, *J. Chem. Phys.* **92,** 6347–6364 (1990).
3. A. Schmidt and S. Vega, The Floquet theory of nuclear magnetic resonance spectroscopy of single spins and dipolar coupled spin pairs in rotating solids, *J. Chem. Phys.* **96,** 2655–2680 (1992).
4. T. Nakai and C. A. McDowell, An analysis of NMR spinning sidebands of homonuclear two-spin systems using Floquet theory, *Mol. Phys.* **77,** 569–584 (1992).
5. T. Nakai and C. A. McDowell, Application of Floquet theory to the nuclear magnetic resonance spectra of homonuclear two-spin systems in rotating solids, *J. Chem. Phys.* **96,** 3452–3466 (1992).
6. A. E. Bennett, R. G. Griffin, and S. Vega, Recoupling of homo- and heteronuclear dipolar interactions in rotating solids, *in* "Solid-State NMR IV: Methods and Applications of Solid-State NMR" (B. Blümich, Ed.), pp. 1–78, NMR Basic Principles and Progress, Vol. 33, Springer-Verlag, Berlin (1994).
7. B. H. Meier and W. L. Earl, A double-quantum filter for rotating solids, *J. Am. Chem. Soc.* **109,** 7937–7942 (1987).
8. D. P. Raleigh, M. H. Levitt, and R. G. Griffin, Rotational resonance in solid state NMR, *Chem. Phys. Lett.* **146,** 71–76 (1988).
9. N. C. Nielsen, F. Creuzet, R. G. Griffin, and M. H. Levitt, Enhanced double-quantum nuclear magnetic resonance in spinning solids at rotational resonance, *J. Chem. Phys.* **96,** 5668–5677 (1992).
10. T. Karlsson, M. Helmle, N. D. Kurur, and M. H. Levitt, Rotational resonance echoes in the nuclear magnetic resonance of spinning solids, *Chem. Phys. Lett.* **247,** 534–540 (1995).
11. Y. Tomita, E. J. O'Connor, and A. McDermott, A method for dihedral angle measurement in solids: Rotational resonance NMR of a transition-state inhibitor of triose phosphate isomerase, *J. Am. Chem. Soc.* **116,** 8766–8771 (1994).
12. P. R. Costa, B. Sun, and R. G. Griffin, Rotational resonance tickling: Accurate internuclear distance measurement in solids, *J. Am. Chem. Soc.* **119,** 10821–19830 (1997).
13. M. Baldus and B. H. Meier, Total correlation spectroscopy in the solid state. The use of scalar couplings to determine the through-bond connectivity, *J. Magn. Reson. A* **121,** 65–69 (1996).
14. A. Kubo and C. A. McDowell, One- and two-dimensional ^{31}P cross-polarization magic-angle-spinning nuclear magnetic resonance studies on two-spin systems with homonuclear dipolar and *J* coupling, *J. Chem. Phys.* **92,** 7156–7170 (1990).
15. S. Dusold, J. Kümmerlen, and A. Sebald, A ^{31}P NMR study of solid compounds $M_xP_2O_7$, *J. Phys. Chem. A* **101,** 5895–5900 (1997).
16. S. Dusold, E. Klaus, A. Sebald, M. Bak, and N. C. Nielsen, Magni-

tudes and relative orientations of chemical shielding, dipolar, and *J* coupling tensors for isolated ^{31}P–^{31}P spin pairs determined by iterative fitting of ^{31}P MAS NMR spectra, *J. Am. Chem. Soc.* **119,** 7121–7129 (1997).

17. G. Wu, B. Sun, R. E. Wasylishen, and R. G. Griffin, Spinning sidebands in slow-magic-angle-spinning NMR spectra arising from tightly *J*-coupled spin pairs, *J. Magn. Reson.* **124,** 366–371 (1997).
18. T. Nakai and C. A. McDowell, Characterization of homonuclear spin pairs from two-dimensional spin–echo NMR powder patterns, *J. Am. Chem. Soc.* **116,** 6373–6383 (1994).
19. K. Eichele, G. Wu, and R. E. Wasylishen, Unusual "AB" spectra in high-resolution magic-angle-spinning NMR studies of solids, *J. Magn. Reson. A* **101,** 157–161 (1993).
20. Note that Eq. (7) given in Ref. (*16*) for C_2 symmetry is incorrect (Eq. (8) in Ref. (*16*), referring to a mirror plane, is correct).
21. M. Edén, Y. K. Lee, and M. H. Levitt, Efficient simulation of periodic problems in NMR: Application to decoupling and rotational resonance, *J. Magn. Reson. A* **120,** 56–71 (1996).
22. M. Edén and M. H. Levitt, Computation of orientational averages in solid state NMR by Gaussian spherical quadrature, *J. Magn. Reson.* **132,** 220–239 (1998).
23. See references given in refs. (*22*) and (*24*).
24. M. Bak and N. C. Nielsen, REPULSION, A novel approach to efficient powder averaging in solid-state NMR, *J. Magn. Reson.* **125,** 132–139 (1997).
25. E. P. Chong and S. H. Zak, "An Introduction to Optimization," Wiley, New York (1996).
26. F. James and M. Roos, MINUIT computer code; Program D-506, CERN, Geneva (1977).
27. W. S. McDonald and D. W. J. Cruickshank, A Reinvestigation of the Structure of $Na_4P_2O_7 \cdot 10H_2O$, *Acta Crystallogr.* **22,** 43–48 (1967).
28. S. J. Kohler, J. D. Ellet, and M. P. Klein, ^{31}P NMR chemical shielding tensors of α-$Ca_2P_2O_7$, *J. Chem. Phys.* **64,** 4451–4458 (1976).
29. P. N. Tutunjian and J. S. Waugh, Electron-coupled spin–spin coupling tensor for ^{31}P in tetraethyldiphosphine disulfide, *J. Chem. Phys.* **76,** 1223–1226 (1982).
30. There is a typographical error in Ref. (*15*): the entry in row one for α [deg] should be -116 ± 1.
31. R. J. Iuliucci, J. Kümmerlen, B. H. Meier, and A. Sebald, to be published.
32. S. Dusold and A. Sebald, Determination of magnitudes and orientations of interaction tensors from MAS NMR spectra of isolated three-spin systems ABX, *Mol. Phys.,* in press.
33. M. D. Lumsden, R. E. Wasylishen, and J. F. Britten, Anisotropy in the ^{199}Hg–^{31}P indirect spin–spin coupling tensor of a 1:2 mercury–phosphine complex. A phosphorus single-crystal NMR study, *J. Phys. Chem.* **99,** 16602–16608 (1995).
34. C. Marichal and A. Sebald, Anisotropy of $^2J(^{119}Sn, ^{117}Sn)$ determined by off-magic-angle spinning ^{119}Sn NMR, *Chem. Phys. Lett.* **286,** 298–304 (1998).
35. R. Challoner and A. Sebald, A double-quantum ^{119}Sn rotational-resonance study, *J. Magn. Reson. A* **122,** 85–89 (1996).
36. G. M. Sheldrick, SHELXTL-PLUS V4.2, Crystallographic System, Siemens Analytical X-ray Instruments, Inc., Madison, WI (1992).
37. M. H. Levitt, The signs of frequencies and phases in NMR, *J. Magn. Reson.* **126,** 164–182 (1997).
38. U. Haeberlen, High resolution NMR in solids. Selective averaging, *in* "Advances in Magnetic Resonance" (J. S. Waugh, Ed.), Supplement 1, Academic Press, New York (1976).
39. P. Hodgkinson and L. Emsley, The reliability of the determination of tensor parameters by solid-state nuclear magnetic resonance, *J. Chem. Phys.* **107,** 4808–4816 (1997).
40. S. A. Smith, T. O. Levante, B. H. Meier, and R. R. Ernst, Computer simulations in magnetic resonance. An object oriented programming approach, *J. Magn. Reson. A* **106,** 75–105 (1994).
41. M. H. Levitt and M. Edén, Numerical simulation of periodic NMR problems: Fast calculation of carousel averages, *Mol. Phys.,* in press.
42. M. Stumber, U. Haeberlen, S. Dusold, and A. Sebald, unpublished results.